Seventh International Conference on Computational Fluid Dynamics (ICCFD7), Big Island, Hawaii, July 9-13, 2012

ICCFD7-4103

Large-Eddy Simulation of Unsteady Separation Over a Pitching Airfoil at High Reynolds Number

D. You and W. Bromby
Corresponding author: dhyou@cmu.edu

Carnegie Mellon University, USA.

Abstract: Large-eddy simulation (LES) of turbulent flow over a pitching airfoil at realistic Reynolds and Mach numbers is being performed. Numerical stability at high Reynolds number simulation is maintained using an unstructured-grid LES technology, which obeys high-order conservation principles and employs a global-coefficient subgrid-scale turbulence model. A hybrid implicit-explicit time-integration scheme is employed to provide a highly efficient way to treat time-step size restriction in the separated flow region which is locally refined with dense mesh. The present simulations confirm the stability and effectiveness of the presented numerical schemes for dynamic stall simulations at realistic operating Reynolds and Mach numbers and show the characteristics of flow separation and reattachment processes which are qualitatively congruent with experimental observation.

Keywords: Dynamic Stall, Unsteady Flow Separation, Large-Eddy Simulation.

1 Introduction

Dynamic stall is a nonlinear and unsteady aerodynamic phenomenon resulting in stall delay during a time-dependent motion of an airfoil at angles of attack higher than its static stall angle. Dynamic stall occurs on the retreating blade of a helicopter rotor experiencing a pitching motion which leads to unsteady flow separation followed by load and pitching-moment overshoots. The unsteady flow separation can, in turn, lead to unacceptably large vibratory loads and acoustic noise, and limit forward flight speeds, load, and maneuverability [1]. The unsteady separation is reported to be influenced by the Reynolds and Mach numbers, blade geometry, pitch rate, and freestream turbulence level [2].

Numerous investigations of unsteady separation associated with dynamic stall have been conducted at chord-based Reynolds numbers in the range of $10^3 - 10^7$, at Mach numbers for incompressible to transonic flow, and for a wide variety of blade geometries. Most experimental studies have concentrated on measurements of aerodynamic forces such as the surface pressure and overall loads [3, 4], or on the flow field visualization [5]. Quantitative measurements of the separated flow field and wake around a pitching airfoil have been difficult using experimental techniques, and therefore, have rarely been reported in the literature.

Computational fluid dynamics has become increasingly useful in studying dynamic stall (see Ref. [6] for a review). Computational works have often been performed, especially at practical Reynolds numbers, using the Reynolds-averaged Navier-Stokes (RANS) equations or its unsteady counterpart (URANS) (*e.g.*, Refs. [7, 8]). However, it is known to be challenging for (U)RANS to accurately predict highly unsteady flow involving incipient flow separation, formation and evolution of stall vortices, and reattachment.

The intrinsic capability of large-eddy simulation (LES) for predicting sufficient details of unsteady separating flows has recently been explored by a certain number of researchers. Nagarajan *et al.* [9] and Ghias *et al.* [10] performed LES of dynamic stall over a pitching airfoil and tip-flow of a rotor in hover using structured-grid finite-difference methods on curvilinear coordinates. The Reynolds numbers considered in these simulations were around 10^5, which are substantially below that of a typical helicopter rotor during low-speed maneuvers ($O(10^6)$). However, LES at higher Reynolds numbers has been difficult mainly due to

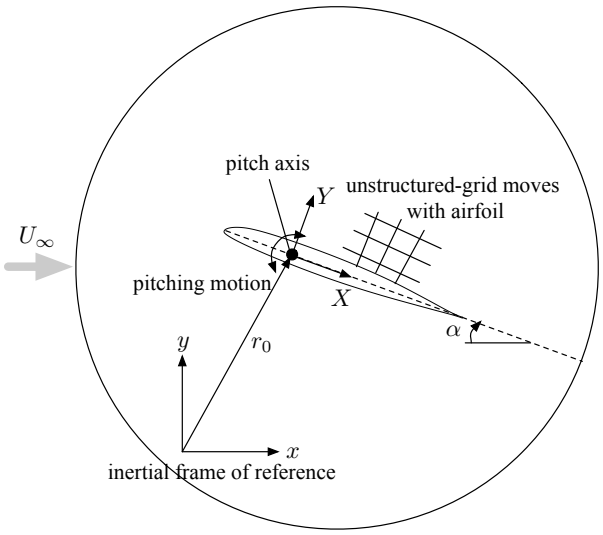

Figure 1: Flow configuration for LES of flow over a pitching airfoil.

the numerical instability issue and high computational costs associated with the spatial and temporal resolution requirements. Simulations and experiments performed at $Re_C < 5 \times 10^5$ indicate that stall frequently occurs when laminar flow separates near the leading edge. This process leads to large steady-state stall hysteresis. However, turbulent separation is more common at high Reynolds number and this makes the unsteady stall characteristics quite dissimilar from the features observed at low Reynolds number. Furthermore, most CFD works including past LES studies so far have focused on the validation of CFD codes and qualitative features of dynamic stall rather than the understanding of the flow physics under realistic flight conditions. Detailed quantitative characterization of velocity and pressure are needed in the separating flow region for the fundamental understanding of the unsteady separation process.

In this work, wall-resolved LES of unsteady separation over a pitching airfoil at realistic Mach and Reynolds numbers is performed. For this purpose, an unstructured-grid LES technology, which maintains numerical stability by obeying high-order conservation principles, is employed. The unstructured grid topology as well as a hybrid implicit/explicit time-integration method provides highly enhanced efficiency in treating spatial and temporal resolution requirements in the dynamically important separated flow region. The research is ongoing with an aim of gaining a quantitative understanding of the unsteady separation process rather than validation and qualitative characterization of the flow field.

2 Flow Configuration

The flow configuration corresponds to an experimental setup in Ref. [3], which was developed to study dynamic stall penetration at constant pitch rate and realistic combinations of Reynolds ($2 - 4 \times 10^6$) and Mach ($0.2 - 0.4$) numbers. The flow configuration models conditions occurring during aircraft post-stall maneuvers and during helicopter high speed forward flight. The blade cross section corresponds to the Sikorsky SSC-A09 airfoil with a chord length of 43.9 cm was installed in the UTRC Wind Tunnel. The surface pressure was measured using miniature transducers, and the locations of transition and separation were determined using surface hot film gages.

Large-eddy simulations of a sinusoidal pitching motion of the airfoil at a reduced frequency, $k = \omega c/2U_\infty = 0.100$, where ω, c, and U_∞ are the angular frequency, chord length, and freestream velocity at Mach numbers of 0.2 and 0.3 and at Reynolds number of 2×10^6, respectively, are being conducted. The computational domain sizes in the radial and spanwise directions are $10c$ and $0.04c$, respectively. Results from ongoing LES will be analyzed in detail with comparisons against experimental data such as aerodynamic forces and moment, surface pressure distributions, and transition and separation locations.

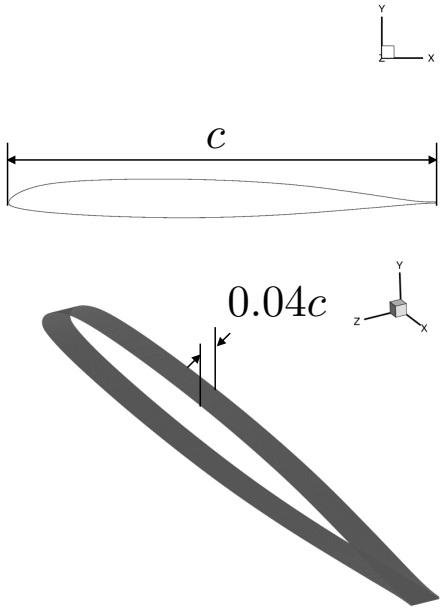

Figure 2: Flow configuration for LES of flow over a pitching airfoil.

3 Numerical Methods

An unstructured-grid LES solver which was developed at the Center for Turbulence Research [11, 12] and which has recently been further developed by You & Moin [13] to include a new subgrid-scale LES model, is employed for the present study. The numerical method is based on unstructured-grid finite-volume discretization of the Favre-filtered compressible Navier-Stokes equations with subgrid-scale stress and heat flux models. The present numerical method overcomes two major difficulties encountered in the previous rotor applications using structured-curvilinear-grid LES approaches [9, 10].

Firstly, it is known that non- or low-dissipative finite-difference schemes on curvilinear coordinates are not strictly conservative [14], and therefore, are more prone to be numerically unstable. Due to the numerical instability, the Reynolds numbers in the previous LES [9, 10] were lower by an order of magnitude ($O(10^5)$) than the practical Reynolds number in rotor applications ($> O(10^6)$). The present Cartesian-coordinate-based finite-volume method maintains the numerical stability as well as the numerical accuracy at high Reynolds number by employing an unstructured-grid spatial-discretization algorithm which is explained as follows:.

The Favre-filtered compressible Navier-Stokes equations can be written as

$$\frac{\partial U}{\partial t} + \frac{\partial F_j}{\partial x_j} = \frac{\partial G_j}{\partial x_j}, \tag{1}$$

where

$$U = \begin{pmatrix} \overline{\rho} \\ \overline{\rho}\widetilde{u}_1 \\ \overline{\rho}\widetilde{u}_2 \\ \overline{\rho}\widetilde{u}_3 \\ \overline{E} \end{pmatrix}, \; F_j = \begin{pmatrix} \overline{\rho}\widetilde{u}_j \\ \overline{\rho}\widetilde{u}_1\widetilde{u}_j + \overline{p}\delta_{1j} \\ \overline{\rho}\widetilde{u}_2\widetilde{u}_j + \overline{p}\delta_{2j} \\ \overline{\rho}\widetilde{u}_3\widetilde{u}_j + \overline{p}\delta_{3j} \\ (\overline{E}+\overline{p})\widetilde{u}_j + \overline{q}_j \end{pmatrix}, \; G_j = \begin{pmatrix} 0 \\ \overline{\sigma}_{1j} - \tau_{1j}^{sgs} \\ \overline{\sigma}_{2j} - \tau_{2j}^{sgs} \\ \overline{\sigma}_{3j} - \tau_{3j}^{sgs} \\ \tilde{u}_k\overline{\sigma}_{jk} - q_j^{sgs} \end{pmatrix}.$$

U is the vector of the Favre-filtered conserved variables and F_j and G_j are the flux vectors in the j-direction. ρ, p, u_i, and E denote density, pressure, velocity component, and energy, respectively. $\overline{\sigma}_{ij}$ and $\overline{q}_j$ are the filtered stress tensor and heat flux, respectively. τ_{ij}^{sgs} and q_j^{sgs} are the subgrid-scale stress tensor and heat flux, respectively.

Finite-volume discretization of the governing equation (1) leads to

$$\frac{\partial U_k}{\partial t} + \frac{1}{V_{\Omega_k}} \sum_f \sum_{j=1}^{3} \left(F_j^f - G_j^f \right) n_j^f = 0, \tag{2}$$

where V_{Ω_k} is the volume measure of a volume-element Ω_k, and U_k is the state variable vector at grid point k. F_j^f and G_j^f are the flux vectors at the element-boundary faces $\partial\Omega_k^f$. n_j^f denotes the face-normal unit vector.

In the present study, the convective and diffusive fluxes are obtained using the *Summation-By-Parts* operators (*e.g.*, skew-symmetric averaging for the convective flux; see also [15]) which guarantee non-growing positive norms of primary variables, thereby maintaining numerical stability. The present method is proven to be particularly well suited for predicting subtle separation effects in turbulent boundary layers at high Reynolds number where boundary layer energetics play a crucial role [11].

In addition, the present LES employes a dynamic *global-coefficient* subgrid-scale (SGS) model which has recently been developed by You & Moin [13]. In the dynamic Smagorinsky model [16, 17], which has widely been used in LES, the model coefficient is dynamically determined as a function of space and time using the scale-invariance concept and the *local-equilibrium* hypothesis (*i.e.,* an equilibrium between the subgrid-scale dissipation and the viscous dissipation at the same physical location). Although the dynamic model coefficient vanishes where the flow is laminar or fully resolved, it can cause numerical instability since its value often becomes negative and/or highly fluctuates in space and time.

To overcome the deficiency of the dynamic Smagorinsky model, You & Moin developed a dynamic procedure for determining the model coefficient utilizing a *global equilibrium* between the subgrid-scale dissipation and the viscous dissipation [13], of which concept was originally proposed by Park *et al.* [18]. In this approach, the model coefficient is globally constant in space but varies in time, and it still guarantees zero eddy viscosity in the laminar-flow regions. The model does not require any *ad hoc* numerical stabilization or clipping operation which is usually necessary in the local-equilibrium based dynamic models.

Secondly, it has been difficult to selectively resolve dynamically important separated flow regions using H- and O-type curvilinear mesh topologies, which are most commonly used in rotor applications. Previous experience with wall-resolved LES of turbulent flows indicates that streamwise and spanwise spacings of about 50–100 and 30–50 wall-units, respectively, are required in the separated flow region and wake. Although local-refinement or overset type grids may be used, it is known that numerical errors associated with the spatial interpolation adversely affect the simulation results. In the present method, the issue is overcome by an unstructured-grid topology, which provides higher flexibility and efficiency in distributing mesh resolution (Fig 3).

Furthermore, the high CFL number restriction in the local dense mesh region is alleviated with the use of a hybrid implicit/explict time-advancement scheme. The discretized governing equation (1) is recast as

$$\frac{\partial U}{\partial t} = H(U), \tag{3}$$

where $U = (U_1^T, U_1^T, U_1^T, \cdots, U_N^T)^T$ is the solution vector and N is the number of grid points. Similarly, the right-hand side $H = (H_1^T, H_1^T, H_1^T, \cdots, H_N^T)^T$ is the flux vector defined as

$$H_k = -\frac{1}{V_{\Omega_k}} \sum_f \sum_{j=1}^{3} \left(F_j^f - G_j^f \right) n_j^f. \tag{4}$$

The right-hand side of equation (3) is decomposed as $H = H^e + H^i$, where H^e and H^i are the explicit and implicit parts of H. The stiffness of H is estimated from eigenvalues of the flux Jacobian matrix J as follows

$$J = \frac{\partial H}{\partial U} = \left[\mathcal{J}^{ij} \right], \quad \mathcal{J}^{ij} = \frac{\partial H_i}{\partial U_j}, \quad i = 1, 2, 3, \cdots, N, \quad j = 1, 2, 3, \cdots, N.$$

Since the computation of eigenvalues is very costly for large-scale simulations, we utilize the Gerschgorin theorem which gives a radius of a disc including all the eigenvalues of the Jacobian matrix, thereby providing maximum allowable time step size for stable zone of an explicit scheme. The decomposed equation is advanced

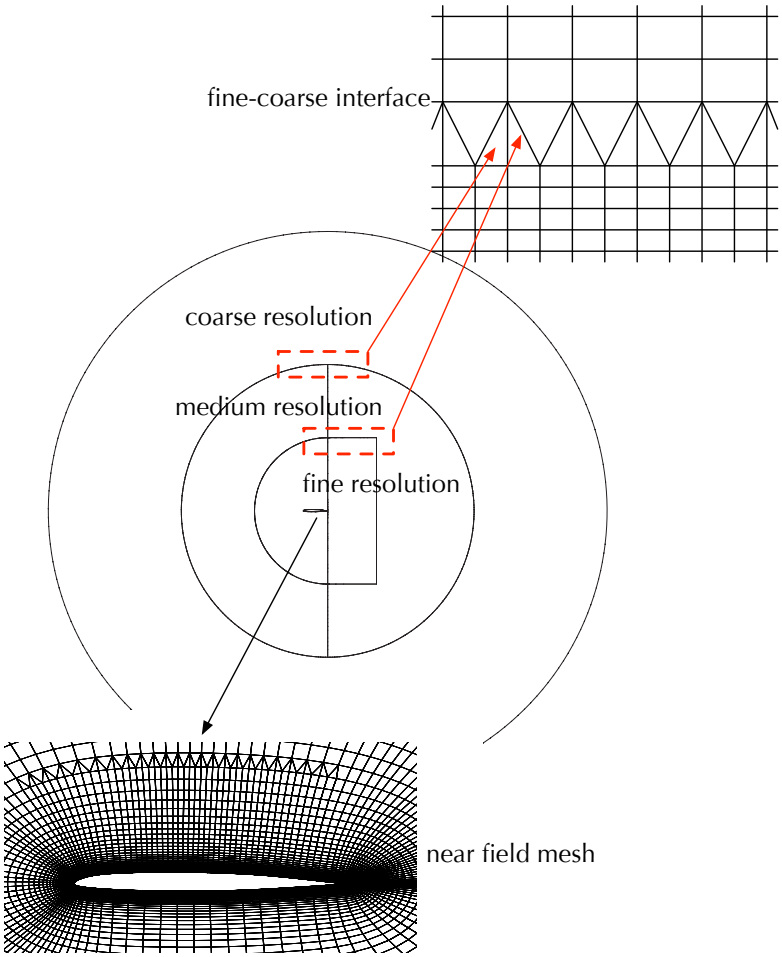

Figure 3: Schematic illustration of the grid resolution topology.

in time using a semi-implicit Runge-Kutta method proposed by Le [19].

This feature allows to adaptively divide the mesh into explicit and implicit zones as shown in Fig. 4 and leads to significantly reduced memory requirements while maintaining the advantage of an implicit integration scheme. This method is especially advantageous for long-time integration of low-pitch-rate unsteady separating flow.

3.1 Results and Discussion

3.1.1 Effects of Mesh Resolution

A series of computational grids were employed to investigate the effects of mesh resolution on the prediction of flow over a steady and pitching airfoils. As discussed in section 2, the present method utilizes advantages of using unstructured grid and adaptive implicit-explicit time-integration scheme. Each grid consists of multiple zones with different grid resolution. Grid lines are clustered around the suction surface of the airfoil and in the wake region so that the separated shear layer, recirculating flow, and turbulent wake are well resolved.

Most of the computational domain is discretized using hexahedral-shape elements. Especially near the airfoil surface, an elliptic-type mesh generator is employed to align grid lines to be parallel and orthogonal to the airfoil surface in the streamwise and wall-normal directions, respectively. As illustrated in Fig. 3, there are numbers of interfaces where mesh resolution is transitioned from fine to coarse. These interfaces

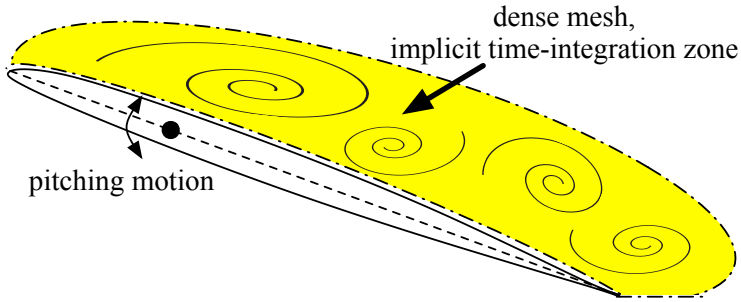

Figure 4: Schematic illustration of the adaptive implicit-explicit time-integration method.

are patched with prism-shape elements to maintain the quality of arrangement of primitive variables.

A mesh with about 6 million cells was designed first and employed for a coarse-resolution LES of flow over a steady airfoil at a fixed angle of attack in order to assess the resolution requirement. Subsequently, a 24 million cell mesh is designed.

Figure 5 shows pressure distributions on the surface of the Sikorsky SSC-A09 airfoil at a fixed angle of attack of 14 degrees. The Reynolds number and Mach number are 2×10^6 and 0.2, respectively. The pressure distribution predicted by the present LES on a 24 million-cell mesh is found to agree well with the experimental measurement in [3]. The near wall resolution in wall units on the 24 million-cell mesh is found to be $\Delta x^+ = 50 - 450$, $\Delta y^+ = 1 - 2$, and $\Delta z^+ = 60 - 130$.

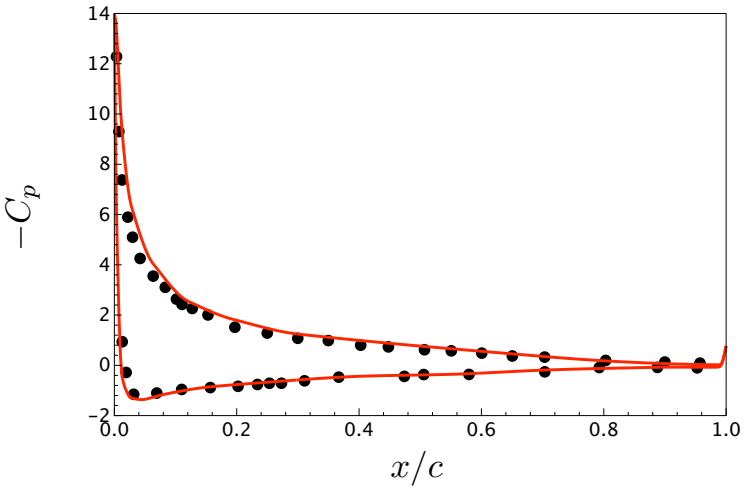

Figure 5: Pressure distribution on the airfoil surface at the angle of attack 14 degrees. Solid line, the present LES solution on a 24 million-cell mesh; symbol, experimental data in [3].

3.1.2 Flow over a Pitching Airfoil

The 24 million cell mesh, which was demonstrated to be reasonably capable of predicting flow over the Sikorsky SSC-A09 airfoil at the operating Reynolds and Mach numbers, is also employed for large-eddy simulations of flow during a pitching motion of the airfoil. To avoid mesh rotation or re-meshing during the pitching motion, the Favre-filtered compressible Navier-Stokes equations are recast into forms in a non-inertial reference frame. Therefore, large-eddy simulations are performed for variables in a non-intertial reference frame along with the effects of the Coriolis, centrifugal, and rotational acceleration forces.

Simulations are ongoing for two different cases. The first case corresponding to an experimental case conducted at Mach number of 0.2 and a sinusoidal pitching motion of which angle of attack varies in time

as follows:

$$\alpha(t) = 20^\circ - 10^\circ \cos(\omega t),$$

where α is the angle of attack as defined in Fig. 1 and ω is the reduced frequency and is $0.10 \times 2U_\infty/c$. The second case also corresponds to an experimental case conducted at Mach number of 0.3 and a sinusoidal pitching motion as follows:

$$\alpha(t) = 12^\circ - 8^\circ \cos(\omega t),$$

where the reduced frequency is identical to the first case.

These two simulations are ongoing while the present simulations confirm the stability and effectiveness of the presented numerical schemes for dynamic stall simulations at realistic operating Reynolds and Mach numbers.

Large-eddy simulations are being conducted with the acoustic Courant-Friedrichs-Lewy (CFL) numbers of 25 and 20 for Mach number of 0.2 and 0.3 cases, respectively. The acoustic CFL numbers correspond to the time-step sizes of 0.27×10^{-3} and 0.23×10^{-3} normalized by the airfoil chord length and the speed of sound for Mach 0.2 and 0.3 cases, respectively. Using 512 cores of SGI Altix ICE 8200LX computer, about 12 - 16 days are required for large-eddy simulation over a pitching period when a 24 million-cell mesh is employed.

The simulations are in progress and Figs. 6 and 7 show gross features of flow over pitching airfoils at two different conditions. The characteristics of flow separation and reattachment processes are qualitatively congruent with experimental observation by Lorber [3].

4 Summary and Future Work

To gain a quantitative understanding of the unsteady separation process over a pitching airfoil, large-eddy simulations (LES) of turbulent flow over a pitching airfoil at realistic Reynolds and Mach numbers are being conducted. A novel combination of discretization schemes and time-integration schemes is employed to achieve numerical stability at high Reynolds number simulations through higher-order conservation and to be equipped with a highly efficient way to treat time-step size restriction in the separated flow region locally refined with dense mesh. The present simulations confirm the stability and effectiveness of the presented numerical schemes for dynamic stall simulations at realistic operating Reynolds and Mach numbers and show the characteristics of flow separation and reattachment processes which are qualitatively congruent with experimental observation.

In the future, systematic analyses of turbulent kinetic energy and vorticity budgets, velocity and pressure fluctuations, spatiotemporal correlations of primitive variables, and the effects of operation parameters, will be performed to gain an understanding of quantitative aspects of dynamic stall. Utilization of the flow-field databases for improving subgrid-scale turbulence models and for developing strategies for dynamic stall control also will be explored.

Acknowledgments

The authors gratefully acknowledge the support of the Army Research Office under Grant No. W911NF1010348, with Dr. Frederick Ferguson as the program manager. Computing time was provided by the National Science Foundation TeraGrid under Grant No. ASC110028 through the Pittsburgh Supercomputing Center and by the U.S. Department of Defense ERDC DSRC.

References

[1] P. F. Lorber and F. O. Carta. Incipient torsional stall flutter aerodynamic experiments on three-dimensional wings. *Journal of Propulsion and Power*, 10(2):217–224, 1994.

[2] W. J. McCroskey. Unsteady airfoils. *Annual Review of Fluid Mechanics*, 14:285–311, 1982.

[3] P. F. Lorber and F. O. Carta. Unsteady stall penetration experiments at high Reynolds number. AFOSR TR 87-1202, April 1987.

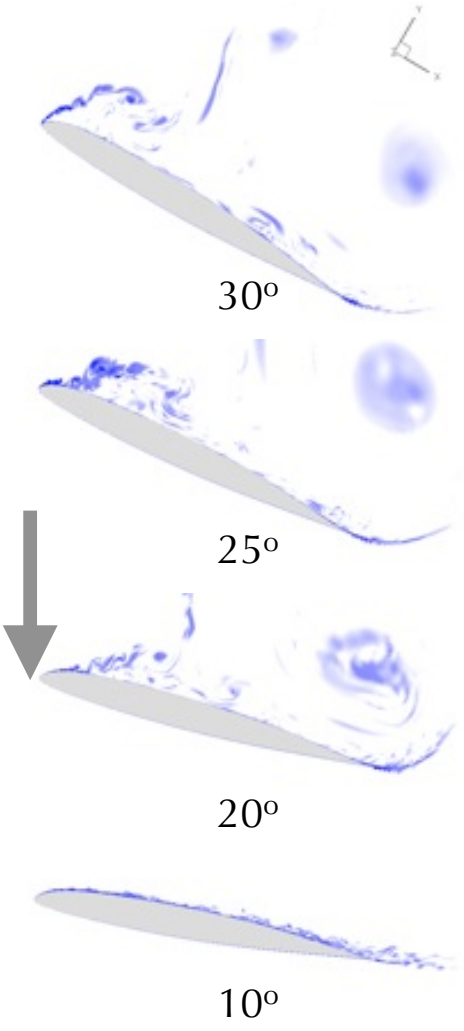

Figure 6: Contours of the spanwise vorticity predicted by the present LES over a half period of pitching motion at Mach number of 0.2.

[4] E. J. Jumper, S. J. Schreck, and R. L. Dimmick. Lift-curve characteristics for an airfoil pitching at constant rate. *Journal of Aircraft*, 24(10):680–687, 1987.

[5] W. J. McCroskey, L. W. Carr, and K. W. McAlister. Dynamic stall experiments on oscillating airfoils. *AIAA Journal*, 14(1):57–63, 1976.

[6] J. A. Ekaterinaris and M. F. Platzer. Computational predictions of airfoil dynamic stall. *Progress in Aerospace Sciences*, 33:759–846, 1997.

[7] M. R. Visbal. Effect of compressibility on dynamic stall of a pitching airfoil. *AIAA Paper 1988-0132*, 1988.

[8] A. Spentzos, G. Barakos, K. Badcock, B. Richards, P. Wernert, S. Schreck, and M. Raffel. Investigation of three-dimensional dynamic stall using computational fluid dynamics. *AIAA Journal*, 43(5):1023–1033, 2005.

[9] S. Nagarajan, S. Hahn, and S. K. Lele. Prediction of sound generated by a pitching airfoil: A comparison of RANS and LES. *AIAA Paper 2006-2516*, May 2006.

[10] R. Ghias, R. Mittal, H. Dong, and T. S. Lund. Study of tip-vortex formation using large-eddy simulation. *AIAA Paper 2005-1280*, January 2005.

[11] D. You, F. Ham, and P. Moin. Discrete conservation principles in large-eddy simulation with application to separation control over an airfoil. *Physics of Fluids*, 20:101515, 2008.

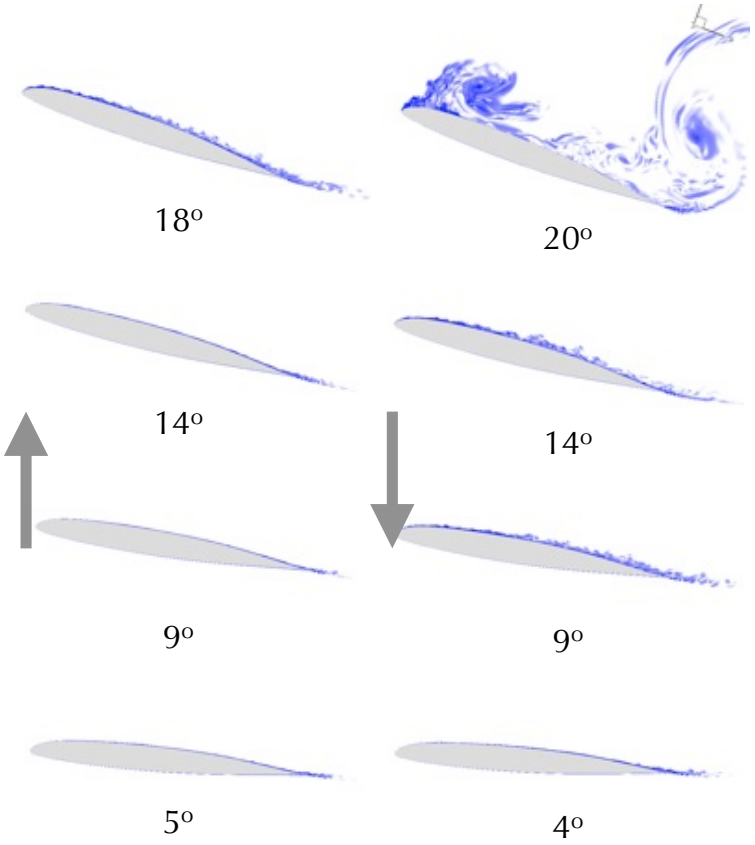

Figure 7: Contours of the spanwise vorticity predicted by the present LES over a period of pitching motion at Mach number of 0.3.

[12] M. Shoeybi, F. Ham, M. Svard, and P. Moin. A stable hybrid implicit/explicit scheme for large-eddy simulation of compressible flows in complex geometries. In *60th Annual Meeting of the Division of Fluid Dynamics*, Salt Lake City, Utah, November 18–20 2007. American Physical Society.

[13] Donghyun You and Parviz Moin. A dynamic global-coefficient subgrid-scale eddy-viscosity model for large-eddy simulation in complex geometries. *Physics of Fluids*, 19(6):065110, June 2007.

[14] S. Nagarajan, J. H. Ferziger, and S. K. Lele. Leading edge effects in bypass transition. TF Report-90, Stanford University, Stanford, California, June 2004.

[15] Bo Strand. Summation by parts for finite difference approximations for d/dx. *Journal of Computational Physics*, 110:47–67, 1994.

[16] M. Germano, Ugo Piomelli, Parviz Moin, and W. H. Cabot. A dynamic subgrid-scale eddy-viscosity model. *Physics of Fluids (A)*, 3(7):1760–1765, 1991.

[17] P. Moin, K. Squires, W. Cabot, and S. Lee. A dynamic subgrid-scale model for compressible turbulence and scalar transport. *Physics of Fluids (A)*, 3:2746, 1991.

[18] Noma Park, Sungwon Lee, Jungil Lee, and Haecheon Choi. A dynamic subgrid-scale eddy-viscosity model with a global model coefficient. *Physics of Fluids*, 18:125109, 2006.

[19] H. Le and P. Moin. An improvement of fractional step methods for the incompressible Navier–Stokes equations. *Journal of Computational Physics*, 92:369–374, 1991.